Tidal range energy resource assessment of the Gulf of California, Mexico.

Carlos Joel Mejia-Olivares[1], Ivan D. Haigh[1], Athanasios Angeloudis[2], Matt J. Lewis[3] and Simon P. Neill[3]

[1] Ocean and Earth Science, National Oceanography Centre, University of Southampton, European Way, Southampton, SO14 3ZH, UK.

[2] School of Engineering, Institute for Infrastructure & Environment, University of Edinburgh, Edinburgh, EH9 3FG, UK.

[3] School of Ocean Sciences, Bangor University, LL59 5AB, UK.

Corresponding author

E-mail address: carlos.mejia-olivares@noc.soton.ac.uk (Carlos Joel Mejia-Olivares).

Ocean and Earth Science, National Oceanography Centre, University of Southampton, European Way, Southampton, SO14 3ZH, U.K.

Submitted to Renewable energy March 2019.

Reviewed version submitted December 2019

2nd-Re-submitted version March 2020

Abstract

There is growing interest in harnessing renewable energy resources in Latin America. Converting the energy of the tides into electricity has the distinct advantage of being predictable, yet the tidal range resource of Latin America is largely unquantified. The northern part of the Gulf of California (GC) in Mexico has a relatively large mean tidal range (4m to 5m), and so could be a potential site for tidal range energy exploitation. A detailed quantification of the theoretical tidal range energy resource was performed using tidal level predictions from a depth-averaged barotropic hydrodynamic model. In addition, a 0-D operation modelling approach was applied to determine the power that can be technically extracted at four key sites. The results show that the annual energy yield ranges from 20 to 50 kWh/m^2, while the maximum values are between 45 and 50 kWh/m^2 in the vicinity of the Gulf of Santa Clara. Within the region, the Gulf of Santa Clara is one of the most promising, delivering a technical annual energy output of 125 GWh (ebb-only generation), 159 GWh (two-way) and 174 GWh (two-way with pumping) within an impoundment area of 10 km^2. This equates to 50%, 40% and 33% of the absolute value power relative to a much-studied reference site (Swansea Bay, UK) that has been under consideration as the world's first tidal lagoon power plant. This study provides the basis for more detailed analysis of the GC to guide selection of suitable sites for tidal range energy exploitation in the region.

Key words: Tidal range energy; resource assessment, annual energy yield, technical power; Gulf of California; Mexico.

Highlights

- Gulf of California (GC, Mexico) theoretical and technical tidal range energy assessment.
- Peak tidal range between 5 and 8 m at sites in the Gulf of California.
- Theoretical annual energy yield estimates in the northern region were ~ 40 to 50 kWh/m^2.
- Gulf of Santa Clara is the prime candidate site for extractable tidal power output in the GC.

1. Introduction

Over the last two decades there has been increased interest in tidal energy exploitation [1]. Tidal energy offers many benefits compared to other sources of renewable energy, particularly because of the regular and predictable nature of ocean tides [2]. There are two forms of tidal energy. Firstly, tidal-stream energy exploits the kinetic energy of tidal currents through the deployment of devices that are able to convert the stream wise velocity of the currents into a rotational torque [2]. Secondly, tidal range energy exploits the potential energy from the water-level differences between two bodies of water, over the rise and fall of the tide, through the use of an impounded area (lagoon or barrage; see [3] and [4]) to create a large water-level difference (between the sea and the impoundment) – to thus direct flow through turbines. The tidal-stream resource of the Gulf of California has been previously quantified [5], but very little is known about the tidal range resource in this near-resonant system.

In this paper we focus on tidal range energy, which has a long history. Tide mills have utilised tidal energy to operate for at least the last 800 to 900 years [6]. However, the first large-scale commercial tidal range energy project was the 240 MW La Rance Tidal barrage in France, commissioned in 1967. Subsequent schemes in operation include Kislaya, Gubska in Russia [7], Lake Sihwa in South Korea [7-9], Jiangxia in China [10] and Nova Scotia in Canada [7]. These schemes involved the construction of large barrages along tidal inlets or bays [11]. There is a host of additional areas that have been identified as appropriate for tidal range energy extraction, and these are summarised in Neill et al. [12]. The bulk of the global tidal range energy resource is distributed among Canada (23%), Australia (30%), UK (13%), France (13%), US (11%), Brazil (5%), South Korea (2%), Argentina (1%), Russia (<1%), India (<1%) and China (<1%) [12]. Overall, it has been estimated that the global annual theoretical potential tidal range energy resource is ~25,880 TWh [12]. There is also increasing scope in utilising small bays and lagoons for tidal energy conversion, such as the proposal for a Swansea Bay tidal lagoon project in the UK [7]. These schemes aim to balance electricity production and the potential hydro-environmental implications of larger tidal barrage schemes that have been considered to-date.

The demand for electricity in Latin America has increased considerably in recent decades due to substantial economic development and population growth [13]. This paper focuses on Mexico, the second largest country in Latin America (after Brazil). Mexico's crude oil reserves ranks within the top 10 in the world [13], and its electric power consumption per capita is

approximately 2,090 kWh, while in comparison in the USA and the UK the electricity power consumption per capita is 12,984 kWh and 5,129 kWh respectively [14]. In 2014, the mean electricity power consumption per capita in the world was reported as 3,128 kWh [14]. In 2012 and 2013, Mexico consumed approximately 260 TWh and 220 TWh of electricity, respectively. 80% of the electricity produced in Mexico is sourced from thermal power plants and, as a result, the country is highly dependent on the combustion of fossil fuels [15]. In 2013, total carbon dioxide (CO_2) emissions from electricity production in Mexico were approximately 133 million metric tons [16]. However, Mexico has set an ambitious goal of generating 35% of its total electricity from renewable sources by 2027, thus reducing its carbon emission footprint [16]. Accordingly, the Mexican government is keen to exploit sustainable energy resources and carry out detailed studies to more accurately identify suitable and viable sites [16]. To date, 19% of Mexico's electricity is generated by renewable energy resources such as solar, wind turbines, biomass, geothermal and hydropower energy [13]. Currently, no electricity is generated in Mexico with either tidal stream or tidal range energy conversion.

In a companion study by Mejia-Olivares et al. [5], a detailed tidal-stream energy resource assessment was conducted for the Gulf of California (hereafter GC) in Mexico (Fig. 1a). Here, we focus on assessing the theoretical and technical tidal range energy resource in the northern part of GC which has a relatively large spring tidal range (7-8m). To-date, two reports [17,18] have identified sites in the GC with significant potential for tidal range energy conversion.

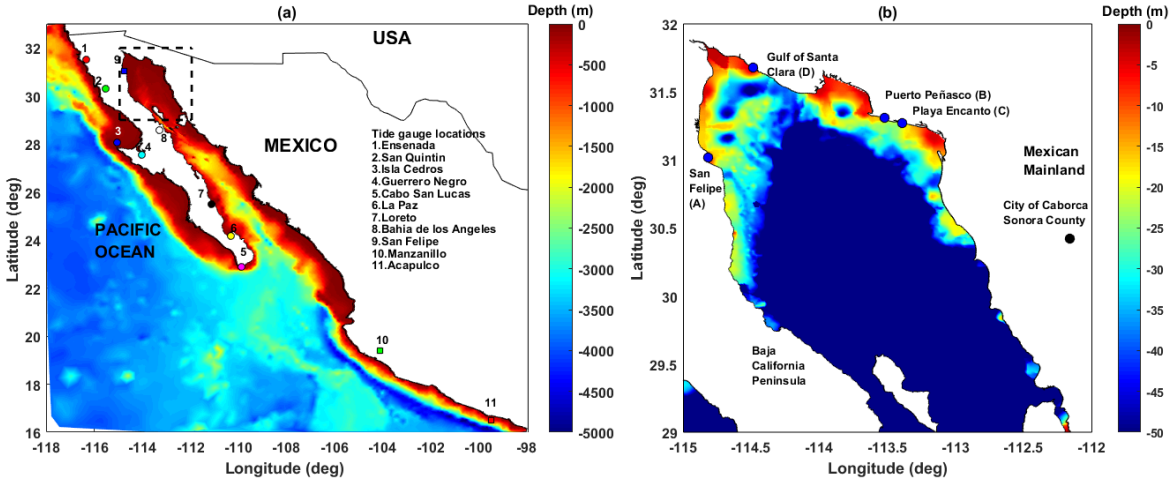

Fig. 1: Location of the study area with bathymetry for the: (a) Gulf of California, with the locations of the tide gauge sites; and (b) the Northern Gulf of California.

Hiriart-Le Bert and Silva-Casarin [17] assessed the potential tidal range energy resource and the feasibility for a tidal barrage situated at San Felipe port in the northern-most reaches of the GC. Using the predictions from a numerical hydrodynamic model (not described in the report cited), they extracted predicted water level time series at San Felipe port, estimating a theoretical annual electricity production of 17,325 GWh, suggesting a basin area of 2,590 km^2. Thus, basin area would have to be impounded by constructing a barrage of more than 72 km in length from San Felipe port at the Baja California Peninsula to Puerto Peñasco (Fig. 1b).

Tapia-Olivas et al. [18] undertook a study identifying several potential sites suitable for tidal range energy extraction, including in the bays of: (i) Santa Maria near San Felipe port, (ii) San Luis Gonzaga southern San Felipe port, (iii) Los Angeles bay, (iv) El Pescador southern Los Angeles Bay, (v) El Soldado at the Bay of las animas, and (vi) San Rafael opposite San Lorenzo Island. Sites (i) and (ii) are situated in the northern reaches of the GC, and (iii) to (vi) are in the Midriff area. In the study by Tapia-Olivas et al. [18] the theoretical tidal range energy resource was estimated using predictions from a three-dimensional numerical model of the GC, configured using the Hamburg Shelf Ocean model (HAMSOM) developed by Backhaus [19] [20] and adapted by [21, 22]. In calculating the resource, they used a theoretical approach and assumed empirical losses due to turbine efficiency. Their results suggested that a 6.87 km^2 impoundment in the Bay of Santa Maria could generate 2.56 MW of power with a total energy extraction of 9.48 GWh/year.

Results from these regional studies indicate that the northern part of the GC has sites with potential for tidal range energy extraction. However, considering the differences in estimated power energy between studies, the need for renewable energy power stations in the region, and recent developments in tidal range power modelling (e.g. [23, 24]), the tidal range resource of the region ought to be more rigorously revisited to understand the potential contribution tidal energy could make to Mexico's renewable energy targets.

The overall aim of this paper is to undertake a detailed quantification of the tidal range energy resource in the northern reaches of the GC. To address this aim there are three objectives, as follows:

1. To map the tidal range distribution in the northern part of the GC;
2. To estimate the theoretical annual potential energy density in this region, and how this resource varies subject to different bathymetry datasets while accounting for multiple tidal constituents; and

3. To determine the available energy that can be technically extracted whilst considering different operational strategies and certain tidal power plant technical specifications. This is accomplished using state-of-the-art operational models that reflect the operation of recent tidal power plant proposals internationally.

The structure of this paper is as follows. After introducing the study region (Section 2), Section 3 provides a brief overview of the model configuration and validation. Section 3 also outlines the methodology used to assess the available power density and theoretical annual energy yield in the northern GC. The results for each of the three objectives are summarized in Section 4. Key findings are discussed in Section 5 and conclusions provided in Section 6.

2. Gulf of California Model Configuration and Validation

This section provides a brief background to the study site, the GC. A general overview of the site is given (Section 2.1) and then the tidal conditions are described (Section 2.2).

2.1 General characteristics

The Gulf of California (GC), a semi-enclosed water basin located to the northwest of Mexico City, is approximately 1100 km long and approximately 45 to 240 km wide and encompasses more than 800 islands. The GC is divided into three parts, Southern (entrance of the Gulf), Central (normally known as Midriff area or Archipelago) and the northern Gulf. The average depth varies from around 200 m in the upper Gulf, to 3,600 m at its connection with the Pacific Ocean (Fig. 1a). It also contains several deep basins, such as Tiburon, Delfin and Wagner which are on average approximately 400, 800 and 200 m deep, respectively (Fig.1b) The Midriff region contains some important Islands, such as Smith, Salsipuedes, San Lorenzo, and San Esteban Islands. The biggest of the Gulf islands are Angel de la Guarda and Tiburon. These Islands form channels, such as Ballenas channel, which is located between the Baja California peninsula and Angel de la Garda Island. The channel is around 14 km and is surrounded by deep water (~800 m). Furthermore, there is a channel between the San Lorenzo and San Esteban Islands (San Lorenzo passage). The northern GC has relatively shallow waters depths ranging from 20 to 200 m depth within Wagner basin (Fig. 1b). The region of most interest to this study is the northern Gulf of California as this is the area with, presumably, the most potential for tidal-range energy exploitation due to its higher tidal range [21].

2.2 Tidal conditions

Understanding and mapping of tides in the GC is fundamental in this study. The Pacific Ocean plays an important role in the generation of tides in the GC which are mainly generated by co-oscillation with low frequencies of tides [25, 26]. The dominant tidal constituents in the GC are the M_2, S_2, K_1 and O_1 constituents [21, 27, 28]. Fig. 2 shows the 3 main semidiurnal and diurnal tidal constituents. The M_2 constituent has an amplitude of around 0.5 m at the entrance of the GC and amplifies to 2.3 m in the northern regions (Fig. 2a), while the S_2 amplitude increases from south to north from 0.2 m to 0.8 m (Fig. 2). The diurnal tidal constituents have lower amplitudes (Fig. 2 d, e and f) and range from 0.05 m to 0.6 m. The amplification of the semidiurnal components occurs because the GC is in near resonance within the principal semidiurnal component, similar to the Bristol Channel in the UK [29-33]. The tides in the GC are mixed; mainly semidiurnal in the southern and northern GC and are mixed mainly diurnal in the Central GC (Figure 2b).

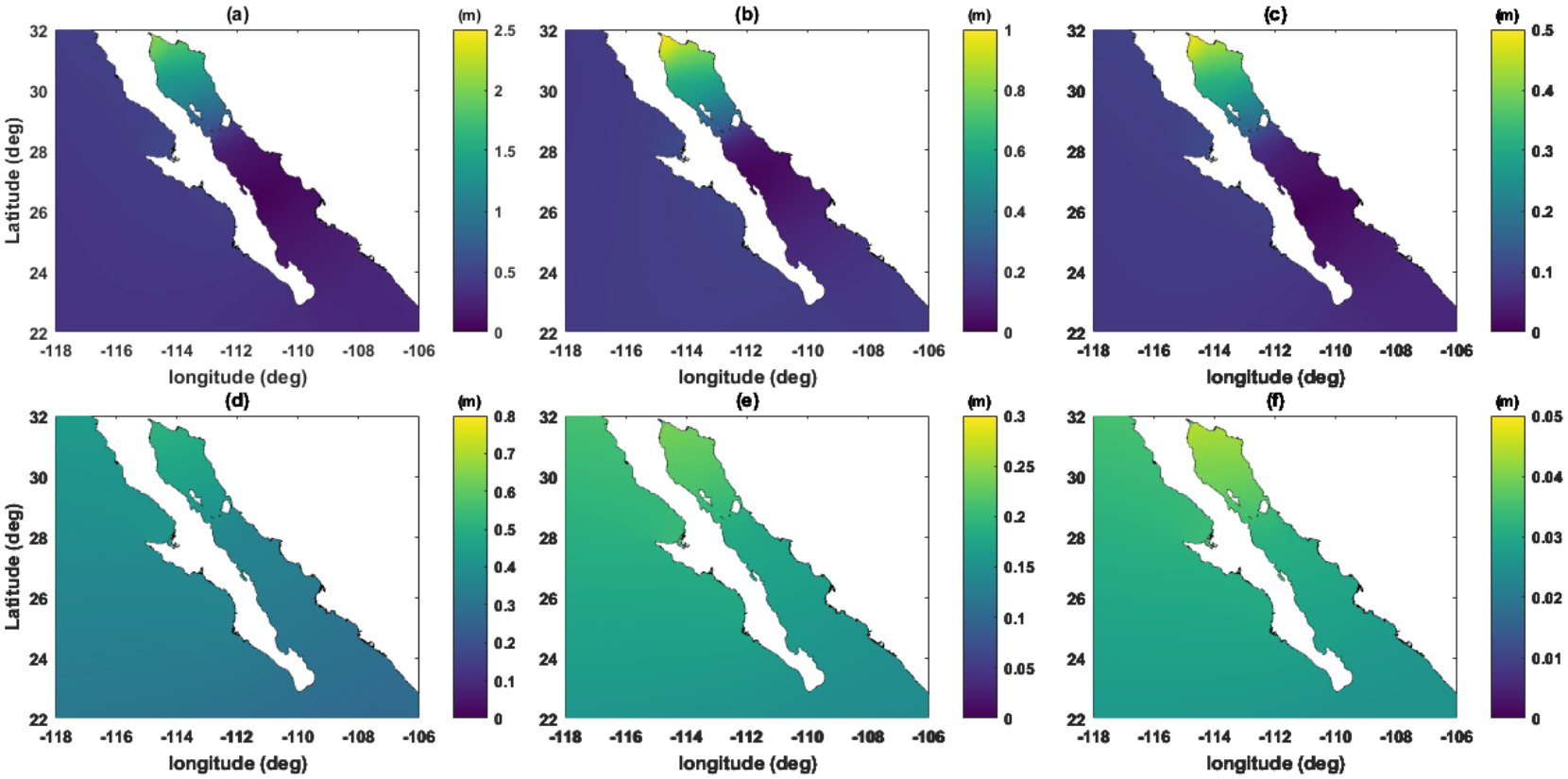

Fig. 2 Amplitude of the main semidiurnal and diurnal tidal constituents: (a) M_2, (b) S_2, (c) N_2, (d) K_1, (e) O_1 and (f) Q_1. Source TELEMAC model described in Section 3.

3. Gulf of California Model Configuration and Validation

We applied a depth-averaged barotropic model for the GC, configured by Mejia-Olivares et al. [5]. Here, we briefly describe the model setup (Section 3.1) and comparisons of model output with measured water level data (Section 3.2); but also direct the reader to the more detailed description of the model configuration and validation provided in [5].

3.1 Model configuration

The model was configured using the TELEMAC modelling suite [34]. TELEMAC is a popular model choice for tidal energy resource assessment characterization, mainly, due to the variable mesh resolution (e.g., [35], [36] and [37]). The generated model mesh has a resolution of 0.507° (~60 km) along the open boundary in the Pacific (Fig. 3a) and increases to 1/120° (~1 km) along the coastline in the northern reaches of the GC (Fig. 3b). The bathymetry data interpolated onto the mesh was downloaded from the General Bathymetry Chart of the Oceans (GEBCO) [38] at a 30 arc-second resolution (~900 m). Higher resolution (~450 m) bathymetry data in the northern GC (obtained from the Centre for Scientific Research and Higher Education at Ensenada; CICESE; (http://www.cicese.edu.mx)), was merged within the GEBCO gridded data (both relative to mean sea level). As a sensitivity test we ran simulations with the bathymetry defined just using GEBCO and then another using ETOPO bathymetry data [39], and this is discussed later in the paper. The open ocean boundary was driven with tidal levels derived from the Oregon State University Tidal Inversion Software (OTIS) TPXO 7.2 database [40] [41] using eight principal (M_2, S_2, N_2, K_2, K_1, O_1, P_1, Q_1), three non-linear (M_4, MS_4, MN_4) and two long period (Mf, Mm) tidal constituents. A constant spatial uniform Manning's friction number of 0.030 $s/m^{1/3}$ was used.

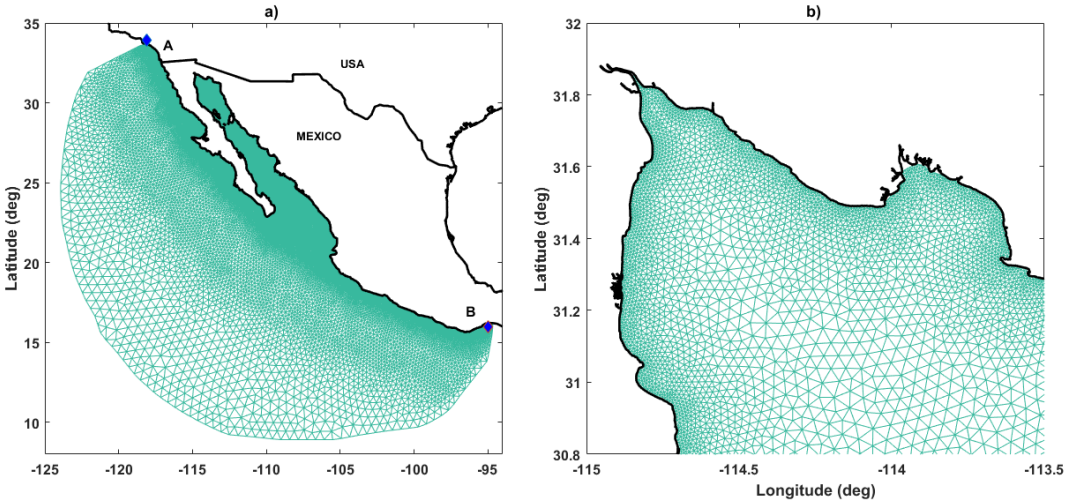

Fig. 3: (a) Domain area model of the Gulf of California (b) Northern GC

3.2 Model Validation

The model has been extensively validated against tide gauge and ADCP measurements to ensure hydrodynamic conditions are accurately reproduced in the GC (see reference [5] for detailed description). Predicted tidal levels were compared against measured water levels at 11 tide gauge sites in the region, the locations of which are shown on Fig. 1a. The tide gauge datasets were obtained from CICESE. We undertook a harmonic analysis of the tide gauge records using T_TIDE [42] to extract the astronomical tidal component. Time-series comparison of the measured and predicted tidal levels are shown in Fig. 4 for December 2015, revealing good agreement at all sites. The largest differences are at La Paz (site 6 in Fig. 1a) which is located in an enclosed bay with a complex bathymetry that is not accurately represented at our present model resolution (3 km in this region).

We calculated the differences between the amplitude and phases of the main tidal constituents and used three error metrics to statistically assess model performance (Table 1) (again see reference [5] for further details). In summary, mean amplitude differences across the 11 validation sites were less than 7 cm for the main constituents, with the exception of K_1 which had an average difference of 20 cm. The mean phase differences were 10° or less for M_2 and O_1, and were below 21° difference for the remaining constituents. For each of the time-series (shown in Fig. 4), the absolute difference between each hourly measured and predicted value was computed. The mean root mean square error (RMSE) and standard deviation of the absolute differences were calculated and correlation coefficients between the measured and

predicted time-series were also derived. The largest RMSE was predicted at Guerrero Negro (0.25 m), while the smallest were at Ensenada (0.03 m), Cabo san Lucas (0.06 m) and Loreto and Manzanillo (0.07 m) (Table 1). The mean standard deviation across the validation sites was 0.078 m, and the mean correlation coefficient was 0.94. In general, this comparison demonstrates that the model performs well in reproducing tidal levels in the GC.

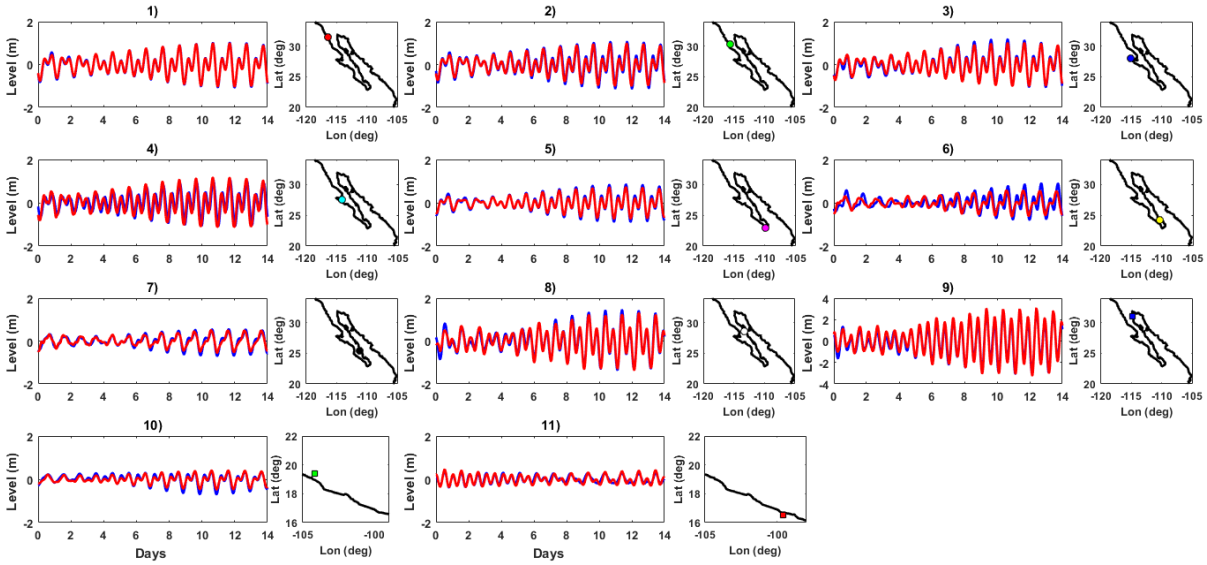

Fig. 4: Comparison of the measured (blue) and predicted (red) tidal time-series at: (1) Ensenada; (2) San Quintin); (3) Isla Cedros; (4) Guerrero Negro; (5) Cabo San Lucas (6) La Paz; (7) Loreto; (8) Bahia de los Angeles; (9) San Felipe; (10) Manzanillo; (11) Acapulco. Reference numbers based on Fig. 1 sites list.

Table 1: Statistical validation error measures for the 11 tide gauge stations including all model tidal constituents of the simulation. See [5] for the time period used for the validation.

Site number	Site Name	RMSE (m)	% Error	STD (m)	Correlation Coefficient
1	Ensenada	0.03	1.2	0.02	0.99
2	San Quintin	0.11	4.5	0.07	0.97
3	Isla Cedros	0.10	4.4	0.09	0.96
4	Guerrero Negro	0.26	9.6	0.15	0.84
5	Cabo San Lucas	0.06	3.0	0.04	0.99
6	La Paz	0.19	10.9	0.12	0.75
7	Loreto	0.08	5.9	0.05	0.95

8	Bahia de los Angeles	0.09	3.0	0.07	0.98
9	San Felipe	0.25	3.8	0.17	0.99
10	Manzanillo	0.07	6.1	0.05	0.94
11	Acapulco	0.07	7.7	0.05	0.91
All	**Mean**	**0.11**	**5.0**	**0.07**	**0.86**

We assessed the sensitivity of the model predictions to bathymetry. To do this, the model was run for three scenarios over a 30-day period in December 2015, using bathymetry data from two sources: (1) GEBCO_2014 [38]; and (2) ETOPO [39], which are available at resolutions of ~900 m and ~775 m, respectively. A third run used GEBCO data merged with higher resolution data from CICESE. Percentage errors between predicted and measured tidal levels were calculated, for each of the three different bathymetries, at each of the 11 tide gauge stations and listed in Table 2.

Table 2. Statistical percentage errors measure of tidal level constituents for the 11 tide gauges stations using different bathymetry datasets considering all the tidal constituents mentioned in section 3.

Site number	**Site Name**	**Error (%)**		
		GEBCO	**ETOPO**	**GEBCO merged with CICESE**
1	Ensenada	1.16	1.2	1.2
2	San Quintin	4.4	4.8	4.5
3	Isla Cedros	4.3	4.5	4.4
4	Guerrero Negro	9.4	8.9	9.6
5	Cabo San Lucas	2.10	2.7	3.0
6	La Paz	11.2	11.5	10.9
7	Loreto	6.3	4.5	5.9
8	Bahia de los Angeles	7	6.8	3.0
9	San Felipe	5.1	3.3	3.8

10	Manzanillo	6	6	6.1
11	Acapulco	7.4	7.4	**7.7**
All	**Mean**	**5.4**	**5.6**	**5.0**

4. Methodology for resource characterisation

In this section, we describe how we used the validated model to assess tidal levels and estimate the energy resources of the region, including undertaking sensitivity tests using different bathymetry sources in the model and varying numbers of tidal constituents to assess sensitivities on the analysis results.

4.1 Tidal level analysis

Tidal levels across the GC were assessed, with a focus on the northern region, to determine the location of the highest tidal range and how it varies over time. The model was run from 27/11/2015 to 31/12/2015 to coincide with time period when observations and results were recorded at every grid point every 10 minutes. The first three days were considered as the warm up period and were discarded from the analysis. At each node, harmonic analysis was conducted on the monthly predicted tidal level time-series using T_TIDE [42]. We then used the tidal harmonics to predict tidal levels for a full year, which reduced the computational expense in running the relatively high-resolution model for a year. In turn, the annual maximum and mean tidal range from the annual time-series at the element nodes were calculated. We compared this to the maximum and mean tidal range, computed using the combined M_2 and S_2 tidal constituents alone.

4.2 Methodology to assess theoretical energy density and annual energy yield

Sequentially, we quantified the theoretical energy density (per m^2) in the GC. The energy was estimated following the approach of [3] in which the theoretical potential energy is given by:

$$E = \frac{1}{2}\ \rho g A\ H^2 \quad \text{(units in J)} \qquad \text{(EQ1)}$$

where A is the area of the impounded basin, ρ is the density of sea water (1025 kg/m^3), g is the acceleration due to gravity (9.81 m/s^2), and h (in m) is the head, normally defined as the water level differences between HW (high water) and LW (low water) peaks of a tidal elevation time series. The annual energy yield resource per m^2 (E_{annual}) was then calculated as follows:

$$E_{annual} = \sum_{i=1}^{n} \left(\frac{1}{2}\rho g A {H_i}^2\right) \quad \text{(units J)} \qquad \text{(EQ2)}$$

where n is the accumulated water transitions from HW to LW, or LW to HW. The potential energy estimated by Eq. (1) was divided by the impounded area to produce a metric that represents the spatially varying potential energy (i.e., the energy density, as $E = {}^1/_2\,\rho g h^2$ in J/m^2).

In order to calculate the annual energy yield (per m^2) using Eq. (2), the head H was first extracted from each transition from high to low water and vice versa, from the elevation-time-series. In turn it was used to calculate the energy density for each consecutive flood and ebb phase of the tidal cycle, and then accumulated for 1,411 cycles that occur in a year.

Finally, we undertook a series of sensitivity tests in which we estimated and compared the theoretical energy density for time-series derived using all available tidal constituents (analysing monthly tidal predictions with T_TIDE gave 29 tidal constituents) and then just for the main semi-diurnal constituents, M_2 and S_2. We also compared energy estimates from model runs that used: (1) just the GEBCO bathymetry; (2) just the ETOPO bathymetry; and (3) the GEBCO data merged with the higher resolution data from CICESE in the northern part of the GC.

4.3 Methodology to assess the technically extractable energy

The performance of a tidal-range power plant is related to the operational strategy and the design components [12]. Here we aim to provide a first-order estimation of the technical tidal range resource that can be extracted using a 0D modelling approach [3]. This 0-D modelling approach has been applied on several occasions to assess the performance of tidal-range schemes [43], [44], [45], and is based on the principles of continuity as implemented in [46], building on earlier operational modelling studies from [47] and [48]. Operation sequence algorithms dictate the flow through hydraulic structures and by extension (in the case of

turbines) the power produced or consumed (while pumping). There are multiple ways of operating a tidal power plant, as summarised in the schematics of Fig. 5 which were produced using the model parameters summarised in Table 3. For a more detailed description of the ebb-generation and two-way generation, the interested reader is directed towards Angeloudis and Falconer [49] and for two-way generation with pumping see Yates et al. [44].

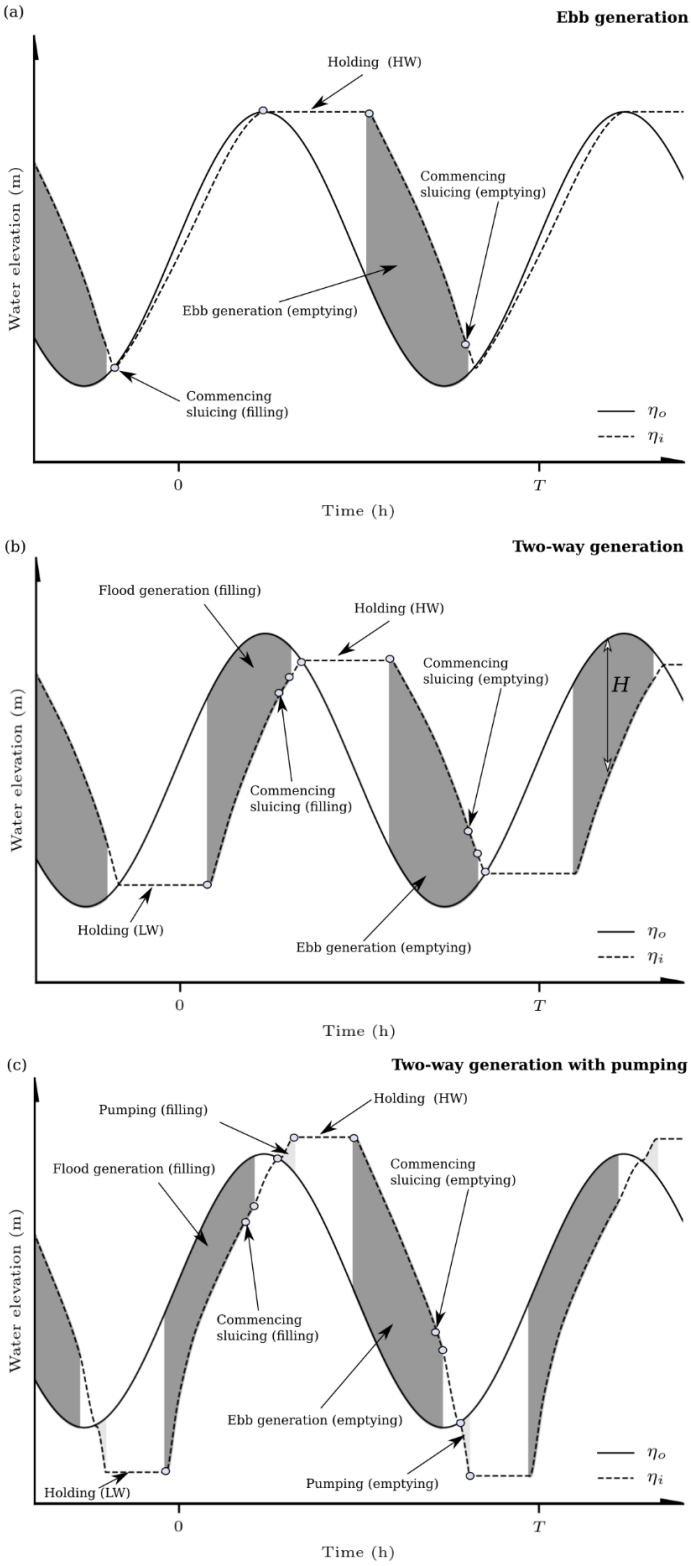

Fig. 5: Typical operation strategies for a tidal range power plant as simulated by the 0-D model: (a) one-way ebb generation, (b) two-way generation and (c) two-way generation with pumping as in [50]. η_o is the outer water elevation in the seaward side of the hydraulic structures while η_i is the inner water elevation within the tidal power plant.

Table 3: Operational parameters used for the 0-D operational model for typical operational strategies employed in tidal range power plants. EBB = One-way ebb generation, TW = Two-way generation, TWP = Two-way generation with pumping.

Operation specifications	**Notation**	**EBB**	**TW**	**TWP**
Holding duration (ebb/flood) (hours)	$t_{h,e}$ / $t_{h,f}$	3.50 / 0.00	3.00 / 3.00	2.00 / 2.00
Pumping duration (ebb/flood) (hours)	$t_{p,e}$ / $t_{p,f}$	0.00 / 0.00	0.00 / 0.00	0.50 /0.50
Max Generation w/o sluicing (ebb/flood) (hours)	$t_{g,e}$ / $t_{g,f}$	6.00 / 0.00	3.00 / 3.00	3.00 / 3.00

Our approach hypothesises the deployment of a tidal lagoon plant at four sites of interest, as follows: Marker A, San Felipe; Marker B, Puerto Peñasco; Marker C, Playa Encanto and Marker D, Gulf of Santa Clara), the locations of which are indicated in Fig. 1b. We selected these four locations as the mean tidal range here exceeded 4 m and the water depths were below 20 m which renders them suitable for the construction of a lagoon while being located close to national electricity grid points, as discussed later in Section 6. A constant upstream surface area of 10 km^2 is assumed as in [48]. This entails a scenario that would be expected for offshore tidal lagoon schemes that would not be influenced by intertidal area (e.g. [51]). As a result, the water volume impounded is assumed to linearly vary with the water depth *h*. The impounded area A = 10 km^2 corresponds to a modest size tidal range scheme. For example, the 320 MW Swansea Bay tidal lagoon project within the Bristol Channel, UK, perceived as a pilot-scale project, has a maximum surface area of 11.6 km^2 [7].

The formulations employed for the flow through hydraulic structures at every time step are outlined in [46] involving the orifice equation for sluice gates using a discharge coefficient of C_D = 1.0 (consistent with the sensitivity study of [52]) and a sluice gate cross-sectional area of A_s = 100 m^2. For the turbine parametrisation, representative hill charts are required to incorporate the performance of low-head bulb turbine designs; this technology is typically installed for power generation from tidal range structure proposals. The calculation process

followed for the hill chart has been described by [53]. In particular, we assume that generation will be facilitated by turbines with a capacity of 20 MW, a diameter D = 7.35 m in accordance with recent UK tidal range energy studies [24], [54], [7]. In Fig. 6 the calculated 20 MW turbine hill chart is plotted together with an idealized representation from first principles. The idealized representation omits efficiency factors acknowledged by the hill chart and demonstrates how lower flows are predicted to generate an equivalent amount of power depending on the head difference H subjected to the turbine. A comparison between the two curves also suggests significant efficiency losses when generating at relatively low head differences; further compromising the generation during neap tides when H would be relatively lower. Moreover, the algorithms account for a minimum head difference that will be required to generate any electricity, where in this case we assume that h_{min} = 1 m.

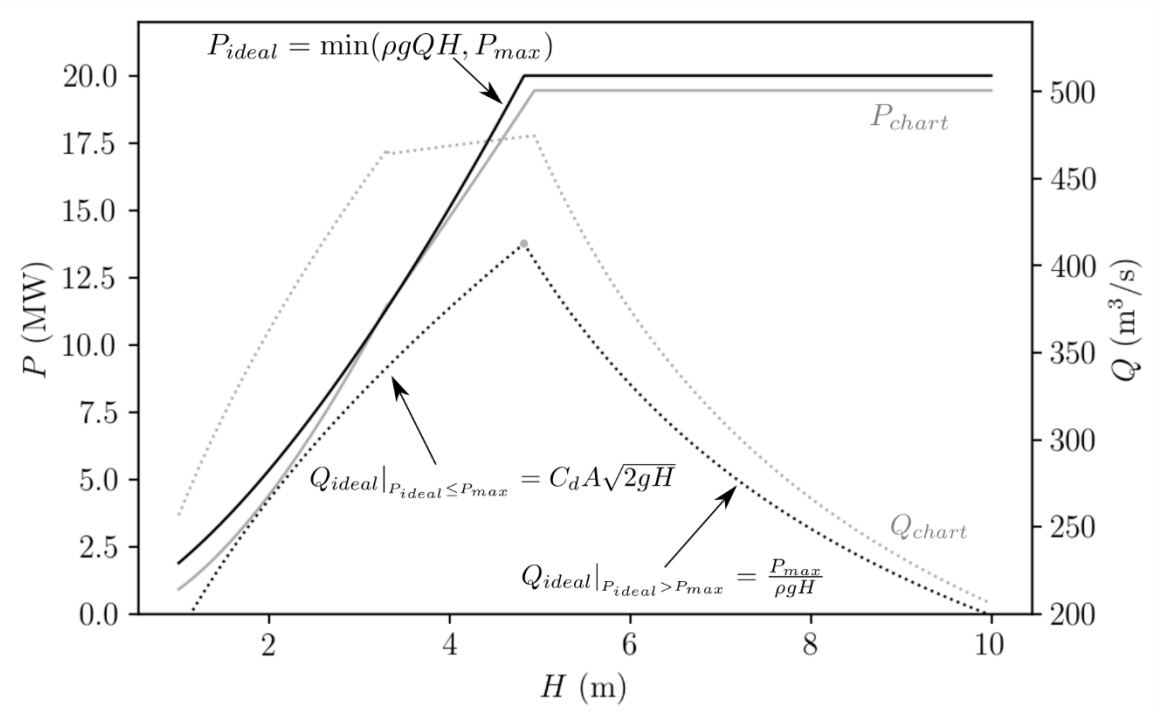

Fig. 6: Idealized and calculated hill chart based on [46]. The hill chart Power (P_{chart}) and Discharge (Q_{chart}) refers to a 20 MW 7.35 m diameter turbine as per the implementation of [46]. For the idealized hill chart, C_d is the discharge coefficient (=1.0), P_{max} = is the turbine capacity (=20 MW) and A_T the cross-sectional area of the turbine (assumed to be = π 7.35^2 /4 m^2) and H the head difference.

In the absence of detailed information about specific schemes at the potential sites in Fig. 1b, certain assumptions must be included in relation to the tidal power plant configuration. Namely, the optimum number of turbines and sluice gates will vary for schemes at different locations according to the available potential energy, amongst additional constraints of a

geomorphological, environmental and electrical nature. For our preliminary assessment we formulate the following expression to estimate the capacity C (in W):

$$C = \eta \frac{\rho g A \bar{H}^2}{T\ CF} \quad \text{(EQ3)}$$

Where η is the overall generation efficiency, T = 44712 s (12.42 h) is the tidal period, CF is the capacity factor and $\bar{H}$ is the mean annual tidal range. It is generally acknowledged that approximately 27 – 55 % of the available energy resource can be harnessed [43], [46]. We thus assume that the maximum potential energy that can be harnessed is subject to an efficiency of η = 0.55. The capacity factor of conventional single-basin tidal range structures can accordingly vary between 0.15 – 0.25 depending on the operation performance. We assume that any proposed scheme in the GC will aim for a value of CF = 0.15. In turn, the number of turbines N_t will be = C/P_{max} and assume for the sluice gate number $N_s = N_t/2$. These parametric relationships have been applied here on an empirical basis, and site-specific optimisation will be essential for more comprehensive practical studies that also acknowledge the site bathymetry, marine spatial planning, economic and environmental constraints.

5. Results

The results of this paper are presented in three parts, each addressing one of the three study objectives (see Section 1).

5.1 Spatial variation in tidal range

The first objective was to map the spatial distribution in tidal range in the northern part of the GC. The annual maximum and annual mean tidal range is shown in Fig. 7a and b, respectively. In the vicinity of the Midriff Islands, the maximum tidal range is in the order of 2 m. The tidal range increases towards the north due to effects of tidal resonance that amplify the tidal wave as it propagates towards the northern coast, facilitating a maximum during spring tides of approximately 8 m in the northern most part of the Gulf (Fig. 7a). The mean tidal range is between 4 to 5 m in the northern most part of the Gulf (Fig. 7b and Table 4 and 5). The annual maximum and annual mean tidal range, calculated using the M_2 and S_2 tidal constituents, are shown in Fig. 7c and d. If we consider the M_2 and S_2 tidal constituents alone, the annual

maximum tidal range reduces significantly from 8 to 5 m in the northern part of the Gulf (Gulf of Santa Clara region), while the annual mean tidal range reduces from 5 to 4 m.

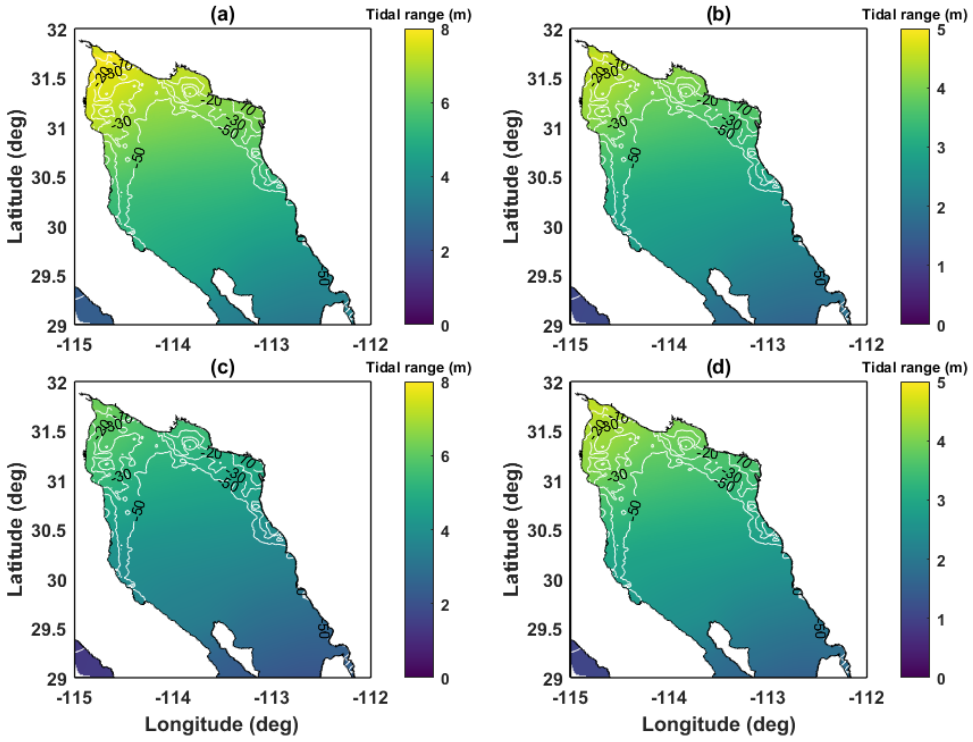

Fig. 7: (a) Maximum tidal range and (b) mean tidal range based on all model constituents, (c) Maximum tidal range and (d) mean tidal range using predicted tide with M_2 plus S_2 tidal constituents. All plots use the GEBCO data merged with the higher resolution data from CICESE, for the northern Gulf of California, with the bathymetry contours overlaid as white lines.

Table 4: Summary of sites considered for operational models in the Gulf of California, and a reference site based on the UK where tidal range projects have been considered. The table summarises, the mean tidal range, the annual energy per unit area, and the installed capacity calculated based on Eq3.

#	Site Name	Latitude (°)	Longitude (°)	$\overline{H}$ (m)	E_{yr}/A (kWh/m^2)	C/A (MW/km^2)
A	San Felipe	31.088	-114.740	4.37	45.2	15.8
B	Puerto Peñasco	31.287	-113.675	4.05	38.6	13.5
C	Playa Encanto	31.264	-113.812	4.08	39.2	13.7

D	Gulf of Santa Clara	31.489	-114.477	4.59	49.8	17.4
Reference	*Swansea Bay*	*51.58*	*-3.90*	*6.61*	*94.7*	*36*

5.2 Energy density and annual theoretical resource

The second objective was to estimate the theoretical potential energy density as well as the theoretical annual energy yield of the region, and how this resource varies subject to different bathymetry datasets while accounting for multiple tidal constituents. The annual maximum and annual mean energy density for an individual transition from High water to Low water in the region is shown in Figs. 8a and b, respectively. Energy density varies spatially and reflects, as expected, the spatial distribution of tidal range, shown in Figs. 8a and b. The maximum values are located at the upper Gulf (opposite the Gulf of Santa Clara) where water depths are less than 30 m and energy density values are around 0.1 kWh/m^2. Moreover, power density is much lower around the Midriff region, ranging from 0.03 to 0.04 kWh/m^2 where water depths vary between 40 and 180 m... Moreover, power density is much lower around the Midriff region, ranging from 0.03 and 0.04 kWh/m^2 where water depths vary between 40 to 180 m. The annual mean energy density for each elevation transition in the upper Gulf is between 0.035 and 0.040 kW/m^2 while in the middle and lower northern GC it is smaller, between 0.025 and 0.018 kW/m^2, respectively as tidal resonance effects are no longer prevalent.

We also estimate the annual maximum and mean power density using predicted tidal level time-series considering just the M_2 plus S_2 tidal constituents and results are shown in Figs. 8c and d. Comparing Fig. 8a with Fig. 8c, the maximum energy density is almost halved when only using considering the M_2 and S_2 tidal constituents, with an indicative reduction from 0.09 to 0.05 kWh/m^2 at the maximum values. Accordingly, the mean energy density reduces from 0.035 to 0.030 kWh/m^2 (Fig. 8b and d).

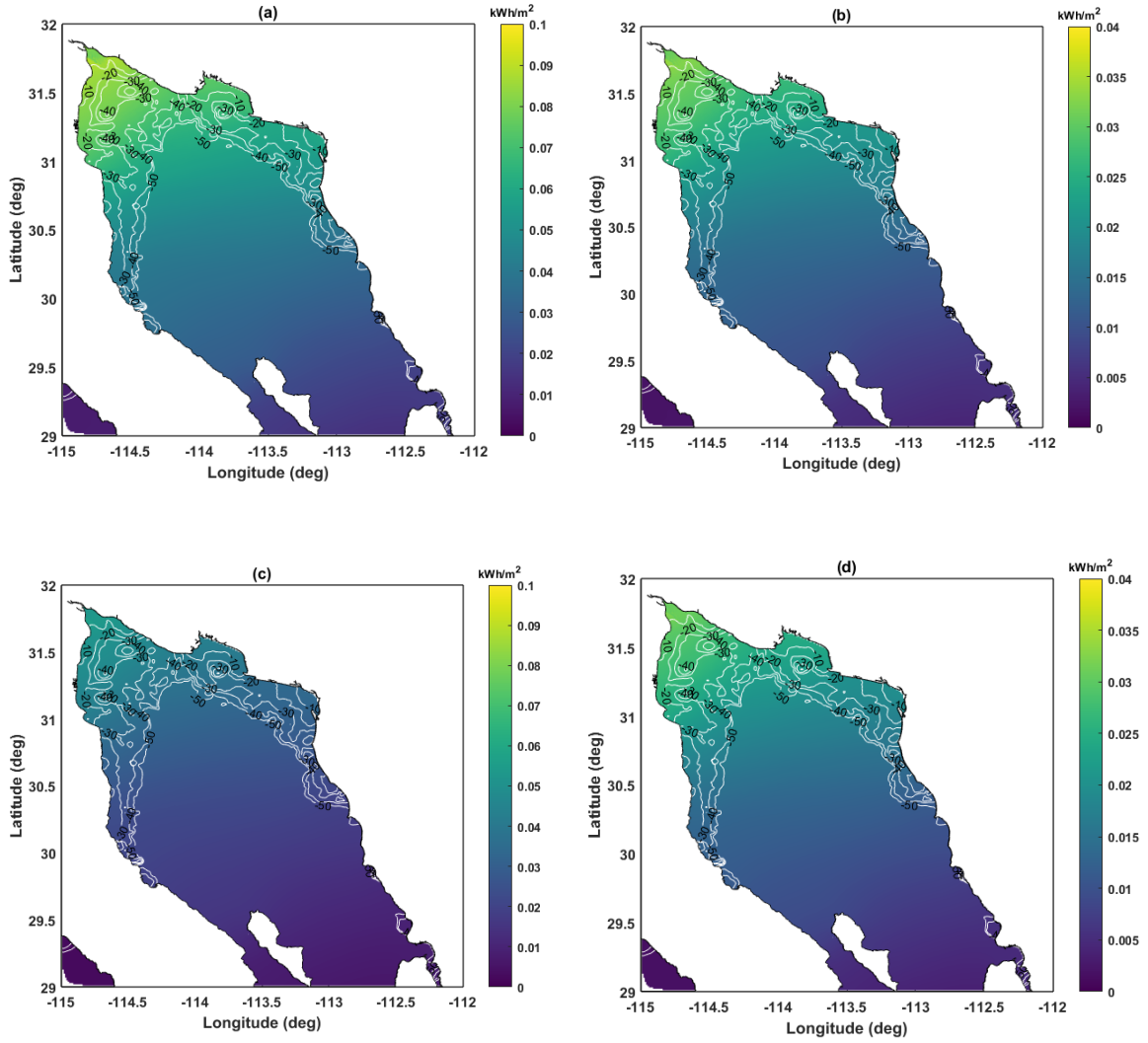

Fig. 8: Maximum energy density based on (a) all model constituents, (c) only M_2 plus S_2 tidal constituents. Mean energy density (b) all model constituents (d) only M_2 plus S_2 tidal constituents. All plots use the GEBCO data merged with the higher resolution data from CICESE, for the northern Gulf of California, with the bathymetry contours overlaid as white lines.

Time series of tidal levels and potential energy density (calculated as instantaneous contributions from each transition from HW to LW and *vice versa)* are shown in Fig. 9a to 9d for four sites in the GC (the locations of which are shown in Fig. 1b). We consider that these areas have potential for constructing a tidal range power plant, as the mean tidal range exceeds 5 m and the topography and water depth are suitable for the construction of a lagoon. The mean annual power density in those locations is in the range of 0.015 to 0.038 kW/m^2.

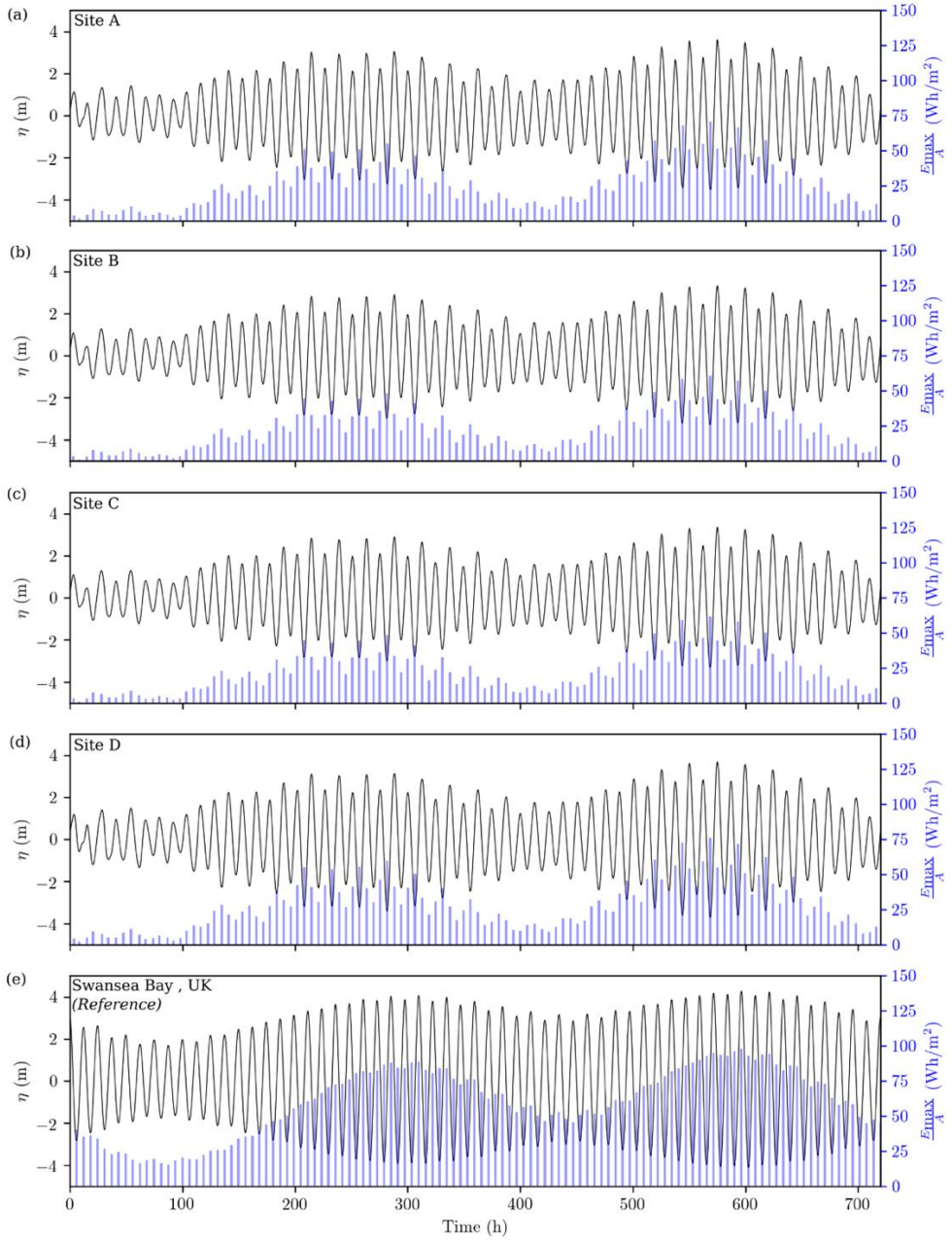

Fig. 9: Monthly energy density and tidal levels at (a) San Felipe, (b) Puerto Peñasco, (c) Playa Encanto, (d) Gulf of Santa Clara and (e) Swansea Bay, UK. The latter is used as a reference for a tidal energy project that has been considered in the Bristol Channel.

We also estimated the theoretical annual energy yield (Fig. 10a). The potential annual energy yield ranges from 20 - 50 kWh/m^2. The maximum values are in the northern region of the GC and are around 45 - 50 kWh/m^2 in the vicinity of the Gulf of Santa Clara. At Puerto Peñasco, San Felipe and Playa Encanto the annual yield energy is lower, ranging from 30 and 35 kWh/m^2. In the southern reaches of the northern GC the annual yield energy is lower, between 20 to 25 kWh/m^2. In a similar way, we compared the annual yield energy based on annual tidal

predictions estimated using only the M_2 and S_2 tidal constituents (Fig. 10b). On average, the resource is 10 to 13 kWh/m^2 higher when considering all 13 tidal constituents analysed, compared to simulations based on M_2 and S_2 alone.

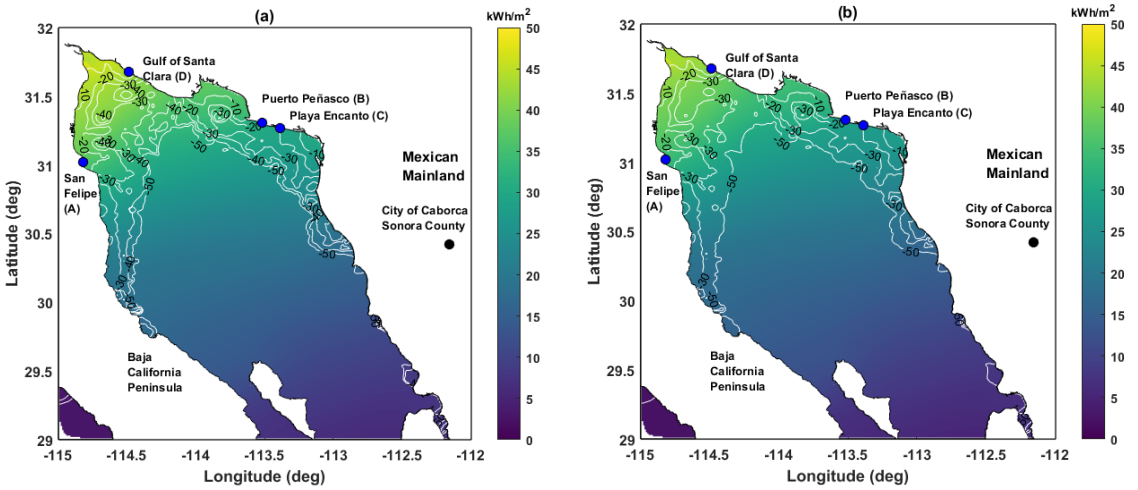

Fig. 10: Annual energy yield (a) all model constituents (b) M_2 plus S_2. All plots use the GEBCO data merged with the higher resolution data from CICESE, for the northern Gulf of California, with bathymetry contours overlaid as white lines.

Three different bathymetry products were used to estimate the theoretical annual energy yield and the contrasting results are shown in Fig. 11. It is clear the resource estimates are underestimated when the GEBCO or ETOPO are used individually. The ETOPO bathymetry gives a maximum resource of 28 kWh/m^2 (Fig. 11b) in the northern region, while the GEBCO bathymetry gives a maximum resource of 20 kWh/m^2 in this area (Fig. 11c). These are around 50% of that estimated when we combine the higher resolution CICESE bathymetry data with GEBCO (Fig.10a).

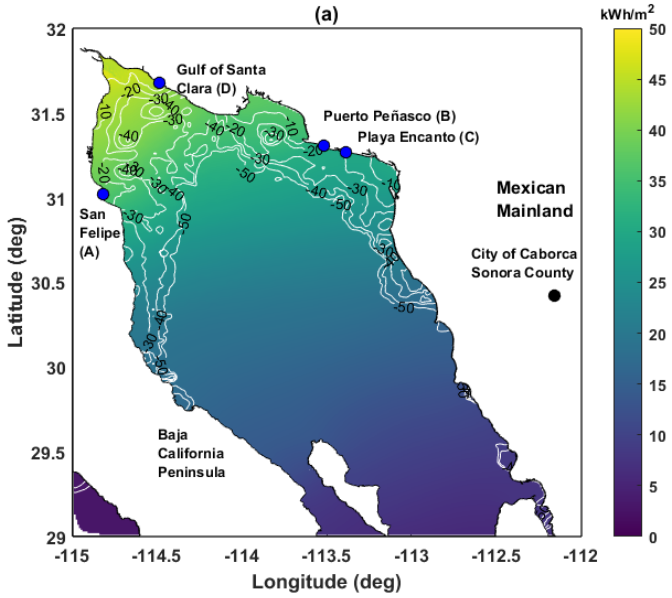
(a)
kWh/m2
Gulf of Santa Clara (D)
Puerto Peñasco (B)
Playa Encanto (C)
Mexican Mainland
San Felipe (A)
City of Caborca Sonora County
Baja California Peninsula
Latitude (deg)
Longitude (deg)

1

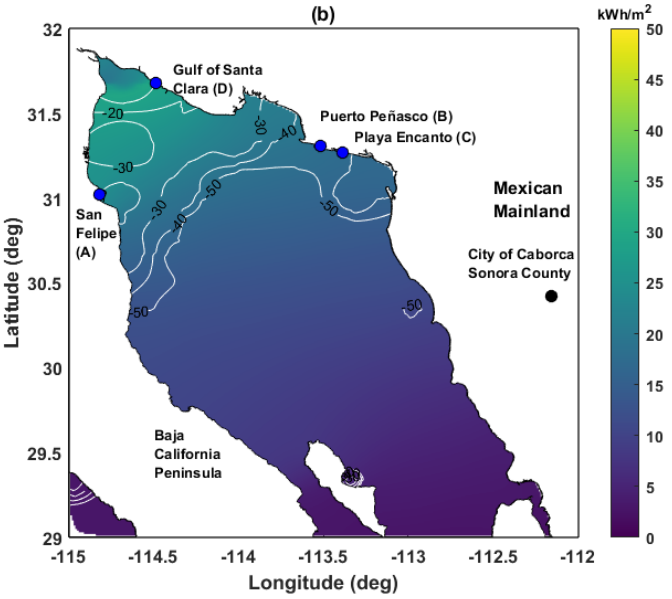
(b)
kWh/m2
Gulf of Santa Clara (D)
Puerto Peñasco (B)
Playa Encanto (C)
Mexican Mainland
San Felipe (A)
City of Caborca Sonora County
Baja California Peninsula
Latitude (deg)
Longitude (deg)

2

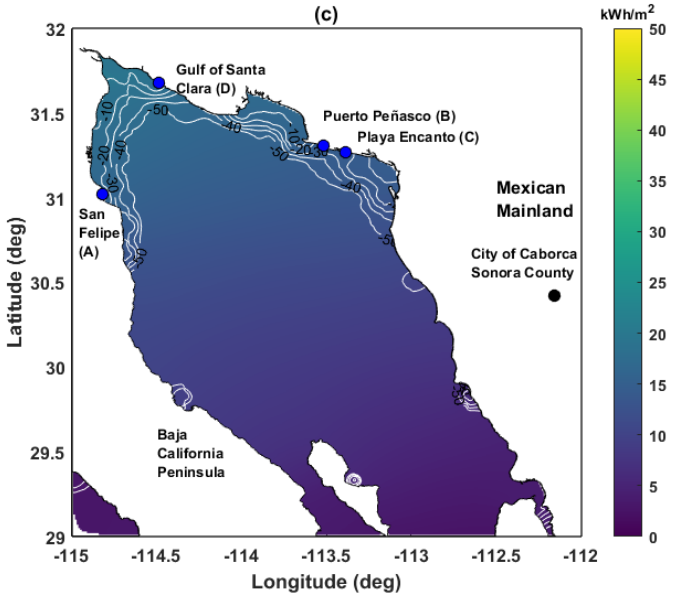

Fig. 11: Annual energy yield using different bathymetry products: (a) GEBCO merged with CICESE (b) ETOPO and (c) only GEBCO with the bathymetry contours overlaid as white lines.

5.3 Technical tidal power output

The third objective was to determine the energy that can be technically exploited whilst considering different operational strategies and certain tidal range power plant technical specifications. In Fig. 9a to 9d we consider the tidal signal and the theoretical energy accumulated in each cycle in sites of interest in the GC. Fig. 9e appends results to be used as a reference based on the theoretical energy from a site where a tidal lagoon proposal has been extensively studied, the Swansea Bay area in the Bristol Channel (UK) [54][55][50]. By observation, the GC is far less energetic in all four locations and this can also be appreciated in Table 5. The tidal range is 30-38% less than for the reference site in the UK. However, this difference corresponds to a 47-59% reduction in the theoretical energy, attributed to the non-linear relationship between tidal range and the available theoretical energy (see Eq. 1).

Table 5: Technical annual energy output and operational efficiency for tidal range energy schemes at selected sites along the coast of the Gulf of California. The table includes results from a reference site in the UK that has been identified as feasible for the deployment of the technology. In all cases the impounded area is = 10 km^2.

#	Site Name	Ebb-only (EBB)		Two-way (TW)		Two-way with pumping (TWP)	
		E_{yr} (Gwh)	η (%)	E_{yr} (GWh)	η (%)	E_{yr} (GWh)	η (%)
A	San Felipe	112	24.8	133	29.7	144	31.9
B	Puerto Peñasco	93	24.1	100	25.9	104	27.1
C	Playa Encanto	94	24.1	103	26.3	108	27.5
D	Gulf of Santa Clara	125	25.1	159	32	174	35
Reference	*Swansea Bay*	*250*	*26.4*	*393*	*41.1*	*520*	*55*

Operational modelling provides further insights into how tidal power plants would perform in the GC. The power output from each of the three strategies is summarised in Fig. 12, where the intervals for power generation can be calculated more accurately. As with every tidal energy technology, considerably less energy is available during neap tidal conditions, with shorter intervals of power generation. One-way operation generates electricity only on the incoming (flood) or outgoing flow (ebb) tide, while two-way operation generates electricity during both periods (ebb and flood) [3]. Two-way generation delivers four pulses of electricity over 24h, which helps distribute the tidal power contributions. Two-way generation with pumping corresponds to improved performance, but this comes with the requirement that energy is invested to pump water and increase the head difference that turbines will then generate [7] from as illustrated in Fig. 12.

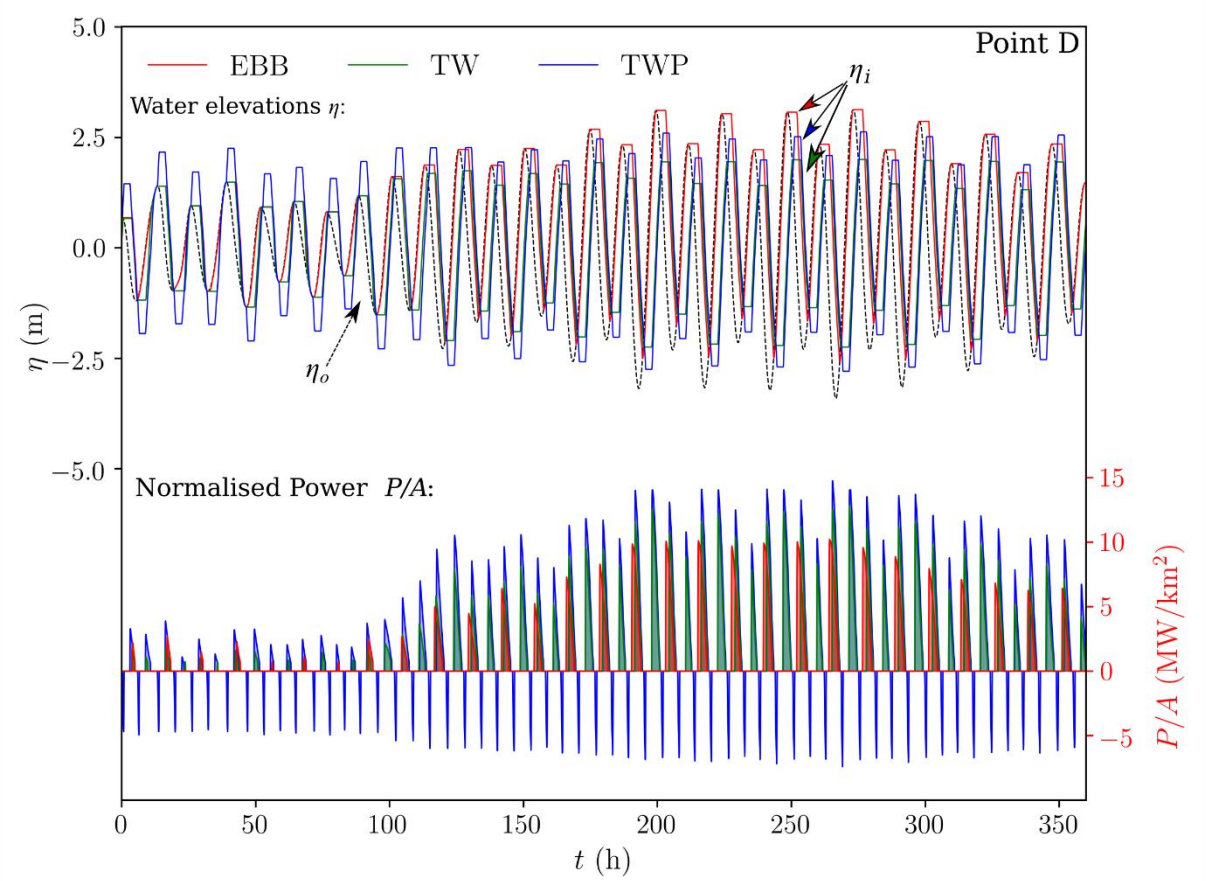

Fig. 12: Water elevations and power produced for the three operational strategies for point D in Fig. 1b (Gulf of Santa Clara). EBB= Ebb-only generation, TW= Two-way generation, TWP = Two-way generation with pumping. η_i = inner water elevations, η_o = outer water elevations. Negative values of power relate to pumping.

Even though it can be observed that energy can indeed be harnessed from the tides in the Gulf of California, there are significant efficiency losses as summarised in Table 5. The power plants consistently perform worse based on the maximum available head at any given site (in this work, the GC in Mexico site relative to the reference one in Swansea Bay). The performance aspect is associated with the head differences between the turbine deployment and the head available at the site. By examining the hill chart in Fig. 6, the efficiency of practical turbine designs increases with an ascending head difference. The lower efficiency can be observed by the significantly greater discharge of Q_{chart} relative to $Q_{ideal.}$, where in the latter hydraulic and other losses are not taken into account. More details on the bulb turbine performance efficiency for tidal range structures can be found in Aggidis and Feather [53]. The best performing site in the GC is the Gulf of Santa Clara (Point D in Fig. 9d & 12) which delivers 50%, 40% and 33% of the energy relative to the reference site for ebb-only, two-way and two-way with pumping strategies respectively.

6. Discussion

In this paper, we have undertaken a detailed quantification of the theoretical and technical tidal range energy resource available in the northern part of the GC. Even though a number of parameters are significant in tidal range energy resource assessments, the most important is clearly tidal range. In this study, we mapped tidal range throughout the GC using results from a validated hydrodynamic numerical model. The annual maximum and mean tidal range is around 8 m and 5 m respectively in the northern most part of the GC, in the vicinity of the Gulf of Santa Clara and San Felipe Bay.

The annual energy density ranges from 20 to 50 kWh/m^2 in the northern part of the GC. The maximum values are between 45 and 50 kWh/m^2 in the vicinity of the Gulf of Santa Clara, where the tidal range peaks. For comparison, the annual energy yield estimated for areas with the world's largest tidal ranges by [12] (e.g. Hudson Bay, Canada; Bristol Channel, UK; Patagonian Shelf; North-western Australian Shelf) is of order 100 kWh/m^2 or more. Also in the study conducted by Neill et al. [12], a minimum acceptable annual yield of 50 kWh/m^2 is suggested, with a maximum water depth of 30 m (based on construction costs of the embankment being prohibitive in deeper waters). In the vicinity of the Gulf of Santa Clara and San Felipe Bay these criteria are just met.

We determined the energy that can be technically converted at four sites at the Upper Gulf of California showed by Marker A, San Felipe; Marker B, Puerto Peñasco; Marker C, Playa Encanto and Marker D, Gulf of Santa Clara, in Fig. 1b. We considered different operational strategies (e.g. flood versus ebb generation) and certain tidal range power plant technical specifications. We contrasted these sites with the proposed tidal lagoon in Swansea Bay in the Bristol Channel of the UK, which has been extensively studied (e.g. [54] [55]). The best performing of the four selected sites in the GC is Gulf of Santa Clara (Point D in Fig. 9d & 12). This site has a technical annual energy output of 125 GWh (ebb-only), 159 GWh (two-way) and 174 GWh (two-way with pumping operational scheme), which corresponds to 50%, 40% and 33% respectively of the absolute power relative to a much studied reference site (Swansea Bay in the UK) utilizing a similar impounded area. In this study we have, for an early-stage assessment, used a 0-D modelling approach. This methodology omits the influence of the structure on the localised hydrodynamics, and assumes a constant impounded surface area with negligible water elevation variations in its interior [3]. The operational algorithms employed in

0-D (Fig. 5) have previously been linked with 2-D hydrodynamic models to quantify hydrodynamic implications associated with the construction of tidal range structures [55], [24] and [56]. Comparisons between the two approaches (0-D and 2-D) suggest that similar findings can be obtained when assessing small-scale projects under certain conditions, and are characterised by a degree of uncertainty due to storm surges [57]. Nevertheless, a positive agreement has been observed for schemes that do not feature extensive intertidal regions upstream [12]. In contrast, caution has been advised for larger schemes such as the Severn Barrage proposal in the UK (impounding approximately 573 km^2, [57]), or for multiple medium-sized schemes operating concurrently. Discrepancies have been reported in the case of designs that occupy significant proportions of estuarine regions that are tidally affected and with a substantial proportion of the impounded area comprising shallow water regions susceptible to extended periods of exposure. Larger impoundments are expected to correspond to a noticeable impact on the estuarine tidal resonance by compromising the established evolution and reflection of the tidal waves, thus markedly altering the downstream tidal conditions that drive the operation and dictate the extractable energy resource. In contrast, schemes that comprise extensive shallow water regions might experience non-linear and rapid surface area changes that would simply not be captured through a 0-D modelling approach.

With regards to the bathymetry data, the results indicate that the percentage error are overall lower for the third run, where GEBCO and CICESE bathymetric datasets are merged. Therefore, including higher resolution bathymetry data places tidal-energy resource of the Gulf of California higher than initial estimates, compared to publicly available/ coarse data products, which has interesting implications for assessments focusing on the potential global resource and tidal energy industry size (e.g. [59]). Also, it is important to mention that the best validation was obtained utilising GEBCO merged with CICESE data sets, consequently we decided to not run a new simulation utilising bathymetry data between ETOPO merged with the bathymetry from CICESE.

As we previously highlighted in relation to tidal-stream energy within the GC study conducted by [5], grid connectivity in the region presents an additional challenge. The nearest electricity connection point to the Mexican national network is located in Sonora County, which is ~450 km from Playa Encanto. North of the GC there are two electricity connection points on the Mexican/US border, but these are not connected to the national Mexican network. These points are located ~200 and ~370 km to San Felipe Bay. Access to this region, due to its topography, lack of fresh water and dry weather make this area unattractive for urban development.

Furthermore, all four selected sites would be closely in phase with one another (Fig. 9a-d). Therefore, the tidal-range energy that could be could be converted into electricity from the GC might be more suitable for off-grid applications (e.g. [60]).

6. Conclusions

The aim of this paper was to undertake a detailed quantification of the tidal range energy resource in the northern reaches of the GC. This study used tidal level predictions from a TELEMAC depth-averaged barotropic hydrodynamic model. The model was validated against tide gauge records, demonstrating a high level of accuracy.

The simulations showed that the maximum tidal range exceeds 8 m in the northern most part of the GC, in the vicinity of the Gulf of Santa Clara and San Felipe Bay. However, the mean tidal range is closer to 5 m in this area. In the northern part of the GC the annual energy density yield ranges from 20 to 50 kWh/m^2. The maximum values are between 45 and 50 kWh/m^2 in the vicinity of the Gulf of Santa Clara, where the tidal range is highest.

We adopted a 0-D modelling approach to estimate the energy that can be technically converted at four sites in the northern GC, considering typical operational strategies and actual tidal range power plant technical specifications. Results showed that the site with the highest energy potential is in the Gulf of Santa Clara which hosts the highest mean tidal range in the GC (4.59 m, approx. 2 m less than the average of Swansea Bay, UK). This site would generate a theoretical annual yield of 49.8 kWh/m^2. Assuming an impounded area of 10 km^2, the annual technical yield of a tidal range power plant becomes 112 GWh (for an ebb flow scheme), to 133 GWh (for a two-way ebb and flood flow scheme), to 144 GWh (for a two-way operational scheme with pumping) indicating capacity factor of 24.8%, 29.7% and 31.9% respectively.

The northern Baja California region presents important challenges to distribute electricity locally as well as exporting electricity throughout the northwest border. Furthermore, in 2015 electricity production figures indicated that the Baja California North has a limited electricity production with only 5% of the national electricity demand (13,122 GWh) [58]. In this region, the best performing sites are in the Gulf of Santa Clara. Here, utilizing two-way generation with pumping could yield 174 GWh/year for a 10 km^2 scheme. Therefore, further studies are recommended for tidal-range energy generation in the Gulf of Santa Clara.

This research has two novel elements. First, it is the most comprehensive assessment of tidal-range energy resource to date for the GC. Two assessments have been conducted prior to this study (e.g., Hiriart-Le Bert et al., 2009; Tapia et al., 2013), but these were very limited in scope. We undertook a more detailed approach, and calculated the theoretical and technical tidal-range energy resource in the upper Gulf, whilst considering different operational strategies and tidal power plant technical specifications. As discussed in the introduction, the Mexico Government has set an ambitious target of generating 35 % of its total energy from renewable sources by 2027 [16]. Presently, 19 % of Mexico's electricity is produced through renewable sources. Tidal energy extraction in the GC would provide a potential source of renewable energy to contribute to this target. Secondly, results from this work can provide a basis for the Mexican Government and policy makers to guide selection of suitable sites for tidal-range energy extraction in the region, and provides a foundation for more detailed assessment.

Acknowledgements

This research was partially financed by CONACyT (the National Council of Science and Technology) through the grant "Becas en el extranjero 2014-1" grant reference CVU 536867 and also by the University of Southampton. A Angeloudis would like to acknowledge the financial support from the NERC (UK's Natural Environment Research Council) grant NE/R013209/1. S.P. Neill and M.J. Lewis acknowledge the financial support of the National Research Network for Low Carbon Energy and the Environment (NRN-LCEE) funded by the Welsh Government and the Higher Education Funding Council for Wales (HEFCW). M.J. Lewis wishes to also acknowledge the EPSRC METRIC grant (EP/R034664/1).

References

[1] Neill, S. P., Hashemi, M. R. Fundamentals of Ocean Renewable Energy: Generating Electricity from the Sea, Academic press. Elsevier 2018.

[2] Bahaj, A. S. 2011. Generating electricity from the oceans. Renewable and Sustainable Energy Reviews, 15, 3399-3416.

[3] Prandle, D., 1984. Simple theory for designing tidal power schemes. Adv. Water Resour. 7, 21–27. https://doi.org/10.1016/0309-1708(84)90026-5

[4] Baker, C., 2006. Tidal Lagoon Power Generation Scheme in Swansea Bay. HM Government, London.

[5] Mejia-Olivares, C. J., Haigh, I. D., Wells, N. C., Coles, D. S., Lewis, M. J. & Neill, S. P. 2018. Tidal-stream energy resource characterization for the Gulf of California, México. Energy, 156, 481-491

[6] Rosario, J., Serrano, J., Carlos Mendoza Sanchez, J. & Vidal, J. 2006. Exploitation of tidal power in the Bay of Cadiz: Ancient tidal mills.

[7] Waters, S. & Aggidis, G. 2016. Tidal range technologies and state of the art in review. Renewable and Sustainable Energy Reviews, 59, 514-529.

[8] Bae, Y. H., Kim, K. O. & Choi, B. H. 2010. Lake Sihwa tidal power plant project. Ocean Engineering, 37, 454-463.

[9] Park, Y. H. 2017. Analysis of characteristics of Dynamic Tidal Power on the west coast of Korea. Renewable and Sustainable Energy Reviews, 68, 461-474.

[10] Zhang, Y.-L., Lin, Z. & Liu, Q.-L. 2014. Marine renewable energy in China: Current status and perspectives. Water Science and Engineering, 7, 288-305.

[11] Charlier, R.H., Forty candles for the Rance River TPP tides provide renewable and sustainable power generation. Renewable and Sustainable Energy Reviews, 2007. 11(9): p. 2032-2057.

[12] Neill, S.P., Angeloudis, A., Robins, P.E., Walkington, I., Ward, S.L., Masters, I., Lewis, M.J., Piano, M., Avdis, A., Piggott, M.D., Aggidis, G., Evans, P., Adcock, T.A.A., Židonis, A., Ahmadian, R., Falconer, R., 2018. Tidal range energy resource and optimization – Past perspectives and future challenges. Renew. Energy 127. https://doi.org/10.1016/j.renene.2018.05.007.

[13] Alemán-Nava, G. S., Casiano-Flores, V. H., Cárdenas-Chávez, D. L., Díaz-Chavez, R., Scarlat, N., Mahlknecht, J., Dallemand, J.-F. & Parra, R. (2014). Renewable energy research progress in Mexico: A review. Renewable and Sustainable Energy Reviews, 32, 140-153.

[14] Worldbank 2018. Electric power consumption (kWh per capita), Mexico. [online].Available https://data.worldbank.org/indicator/EG.USE.ELEC.KH.PC?locations=MX [accessed 06.03.18].

[15] SENER, Secretaria de Energia. 2015. Inventario Nacional de energias renovables, Available at http://inere.energia.gob.mx/publica/version3.2/ [Accessed 10 December 2014].

[16] SENER, Secretaria de Energia. 2013. Estrategia Nacional 2013-2027, Available at http://www.sener.gob.mx/res/PE_y_DT/pub/2013/ENE_2013-2027.pdf [Accessed 10 December 2014].

[17] Hiriart-Le Bert G. and Silva-Casarin R., Tidal Power plan energy estimation. Engineering Institute, Autonomous National University of Mexico. Mexico. 11 (2) 233-245, 2009.

[18] Tapia Olivas, J. C., Ramirez Campbell, H. E. & Gil Samaniego Ramos, M. 2013. Feasibility Analysis for a Tidal Energy Pilot Site in the Gulf of California. V06BT07A087.

[19] Backhaus, J. O., A semi-implicit scheme for the shallow water equation for application to shelf sea modelling, Cont. Shelf Res., 2, 243– 254, 1983.

[20] Backhaus, J.O., 1985. A three-dimensional model for simulation of shelf sea dynamics. Deutsche Hydrographische Zeitschirft 38 (H.4), 164–187.

[21] Marinone, S.G., 2003. A three-dimensional model of the mean and seasonal circulation of the Gulf of California. Journal of Geophysical Research 108 (C10), 3325, doi: 10.1029/2002JC001720.

[22] Marinone, S. G, González, I. and Figueroa, J.M. Prediction of sea surface elevation and currents in the Gulf of California: scales from tides to seasonal. Environmental Modelling & Software, (2009), 24:140-143, doi:10.1016/j.envsof.2008.05.003.

[23] Angeloudis, A., Ahmadian, R., Falconer, R.A., Bockelmann-Evans, B., 2016. Numerical model simulations for optimisation of tidal lagoon schemes. Appl. Energy 165, 522–536. https://doi.org/10.1016/j.apenergy.2015.12.079.

[24] Angeloudis, A., Falconer, R.A., Bray, S., Ahmadian, R., 2016b. Representation and operation of tidal energy impoundments in a coastal hydrodynamic model. Renew. Energy 99, 1103–1115. https://doi.org/10.1016/j.renene.2016.08.004/

[25] Beier, E. (1997). A Numerical Investigation of the Annual Variability in the Gulf of California. Journal of Physical Oceanography - J PHYS OCEANOGR. 27. 615-632.

[26] Ripa, P. (1997). Toward a Physical Explanation of the Seasonal Dynamics and Thermodynamicsof the Gulf of California.

[27] Argote, M. L., Amador, A., Lavin, M. F. & Hunter, J. R. (1995). Tidal dissipation and stratification in the Gulf of California. Journal of Geophysical Research: Oceans, 100, 16103-16118.

[28] Lavin M.F. and S.G. Marinone. (2003), an overview of the Physical Oceanography of the Gulf of California, Department of Physical Oceanography, CICESE, Ensenada Baja California, Mexico.

[29] Fong, S.W. and Heaps, N.S. (1978) Note on quarter-wave tidal resonance in the Bristol Channel (Institute of Oceanographic Sciences Report, 63) Wormley, UK. Institute of Oceanographic Sciences 11pp.

[30] Serhadlıoğluet, S., Adcock, T. A. A., Houlsby, G. T., Draper, S. & Borthwick, A. G. L. (2013). Tidal stream energy resource assessment of the Anglesey Skerries. International Journal of Marine Energy, 3–4, e98-e111.

[31] Liang, D, Xia, J, Falconer, RA, and Zhang, J (2014). "Study on tidal resonance in Severn Estuary and Bristol Channel, "Coastal Engineering Journal, 56(01),1450002.

[32] Adcock, T. A., Draper, S. & Nishino, T. (2015). Tidal power generation – A review of hydrodynamic modelling. Proceedings of the Institution of Mechanical Engineers, Part A: Journal of Power and Energy, 229, 755-771.

[33] Gao, C. & Adcock, T. A. A. (2016). Numerical Investigation of Resonance in the Bristol Channel. The 26th International Ocean and Polar Engineering Conference. Rhodes, Greece: International Society of Offshore and Polar Engineers.

[34] Jean-Michel Hervouet, "Hydrodynamics of Free Surface Flows: Modelling with the Finite Element Method", Wiley Blackwell, April 2007, 360p, ISBN-13: 978-0470035580.

[35] Coles, D. S., Blunden, L. S. & Bahaj, A. S. 2017. Assessment of the energy extraction potential at tidal sites around the Channel Islands. Energy, 124, 171-186.

[36] Cornett A, Noemie Durand, Martin Serrer (2010). 3-D Modelling and Assessment of Tidal Current Resources in the Bay of Fundy, Canada 3rd International Conference on Ocean Energy, 6 October, Bilbao.

[37] Blunden, L. & Bahaj, A., (2006). Initial Evolution of Tidal Stream Energy Resources at Portland Bill, UK. Renewable Energy, 31, pp.121-32.

[38] Kapoor, D.C., (1981). General bathymetric chart of the oceans (GEBCO). Marine Geodesy, 5(1), pp.73–80.

[39] NOAA (2017). ETOPO1 Global Relief Model [online] United States of America. Available from https://www.ngdc.noaa.gov/mgg/global/. [Accessed March 2017].

[40] Egbert, G. D., A. F. Bennet, and M. G. G. Foreman (1994), Topex/Poseidon tides estimated using a global inverse model, Journal of Geophysical Research, 99, 24,821 24,852.

[41] Egbert, G. D. and S. Y. Erofeeva (2002). "Efficient Inverse Modeling of Barotropic Ocean Tides." Journal of Atmospheric and Oceanic Technology 19(2): 183-204.

[42] Pawlowicz R, Beardsley B, Lentz S (2002). Classical tidal harmonic analysis including werror estimates in MATLAB using T_TIDE. Comput Geosci. 28(8):929–37.

[43] Burrows, R., Walkington, I. a., Yates, N.C., Hedges, T.S., Wolf, J., Holt, J., 2009. The tidal range energy potential of the West Coast of the United Kingdom. Appl. Ocean Res. 31, 229–238. https://doi.org/10.1016/j.apor.2009.10.002

[44] Yates, N., Walkington, I., Burrows, R., Wolf, J., 2013. The energy gains realisable through pumping for tidal range energy schemes. Renew. Energy 58, 79–84. https://doi.org/10.1016/j.renene.2013.01.039

[45] Angeloudis, A., Ahmadian, R., Falconer, R.A., Bockelmann-Evans, B., 2016. Numerical model simulations for optimisation of tidal lagoon schemes. Appl. Energy 165, 522–536. https://doi.org/10.1016/j.apenergy.2015.12.079.

[46] Angeloudis, A., Kramer, S.C., Avdis, A., Piggott, M.D., 2018. Optimising tidal range power plant operation. Appl. Energy. https://doi.org/10.1016/j.apenergy.2017.12.052

[47] Aggidis, G. a., Benzon, D.., 2013. Operational optimisation of a tidal barrage across the Mersey estuary using 0-D modelling. Ocean Eng. 66, 69–81. https://doi.org/10.1016/j.oceaneng.2013.03.019

[48] Lewis, M. J., Angeloudis, A., Robins, P. E., Evans, P. S. & Neill, S. P. 2017. Influence of storm surge on tidal range energy. Energy, 122, 25-36.

[49] Angeloudis, A., Falconer, R.A., 2017. Sensitivity of tidal lagoon and barrage hydrodynamic impacts and energy outputs to operational characteristics. Renew. Energy 114, 337–351. https://doi.org/10.1016/J.RENENE.2016.08.033

[50] Harcourt F., Angeloudis A.,Piggott M. (2019). Utilising the flexible generation potential of tidal range power plants to optimise economic value. Applied Energy, 237, 873-884

[51] Cornett, A., Cousineau, J., Nistor, I., 2013. Assessment of hydrodynamic impacts from tidal power lagoons in the Bay of Fundy. Int. J. Mar. Energy 1, 33–54. https://doi.org/10.1016/j.ijome.2013.05.006.

[52] Bray, S., Ahmadian, R., Falconer, R.A., 2016. Impact of representation of hydraulic structures in modelling a Severn barrage. Comput. Geosci. 89, 96–106. https://doi.org/10.1016/J.CAGEO.2016.01.010

[53] Aggidis, G. A. & Feather, O. 2012. Tidal range turbines and generation on the Solway Firth. Renewable Energy, 43, 9-17.

[54] Petley, S., Aggidis, G., 2016. Swansea Bay tidal lagoon annual energy estimation. Ocean

Eng. 111, 348–357. https://doi.org/10.1016/j.oceaneng.2015.11.022.

[55] Angeloudis, A., Piggott, M.D., Kramer, S.C., Avdis, A., Coles, D., 2017. Comparison of 0-D , 1-D and 2-D model capabilities for tidal range energy resource assessments, in: EWTEC 2017. Cork, pp. 1–10.

[56] Vouriot, C., Angeloudis, A., Kramer, S.C, Piggott, M.D. 2018. Fate of large-scale vortices in idealized tidal lagoons. Environmental Fluid Mechanics. https://doi.org/10.1007/s10652-018-9626-4

[57] Xia, J., Falconer, R. A. & Lin, B. 2010. Impact of different operating modes for a Severn Barrage on the tidal power and flood inundation in the Severn Estuary, UK. Applied Energy, 87, 2374-2391.

[58] PRODESEN, 2016. National Electric System Development Program. Energy Alert - National Electric System Development Program (PRODESEN) 2016 -2030.Available from https://www.ey.com/Publication/vwLUAssets/ey-energy-alert-prodesen-2016-2030/%24FILE/ey-energy-alert-prodesen-2016-2030.pdf. [Accessed November 2018].

[59] Neill, S.P. and Robins, P.E. 2019. Global and regional tidal range resource. Proceedings of the 13th European Wave and Tidal Energy Conference (EWTEC), Napoli, 1-6th September 2019.

[60] Neill, S.P., Hashemi, M.R., Lewis, M.J. 2016. Tidal energy leasing and tidal phasing. Renewable Energy, 85, 580-587.